03
Research paper
Doi 10.61892/STP202601108Y
ISSN 2566-4484

STEPGRAD
СТЕПГРАД

Vasil Yordanov, Politecnico di Milano, vasil.yordanov@polimi.it
Alberto Vavassori, Politecnico di Milano, alberto.vavassori@polimi.it
Sadra Zahed Kachaee, Politecnico di Milano, sadra.zahed@mail.polimi.it
Claudia Isabela Saud Mino, Politecnico di Milano, claudiaisabela.saud@mail.polimi.it
Matej Zgela, Politecnico di Milano, matej.zgela@polimi.it
Afshin Moazzam, Politecnico di Milano, afshin.moazzam@polimi.it
Maria Antonia Brovelli, Politecnico di Milano, maria.brovelli@polimi.it

INTEGRATED EARTH OBSERVATION AND DATA-DRIVEN APPROACHES FOR URBAN AIR QUALITY AND THERMAL ENVIRONMENT MONITORING

Abstract:
Urban environments are increasingly affected by air pollution and urban heat island (UHI) effects, requiring integrated monitoring approaches. Within the Space It Up! project, this work presents coordinated research lines combining Earth Observation (EO) data and data-driven methods. The air quality component includes methane screening, multi-source data integration, and Sentinel-5P data gap analysis, while the thermal comfort component focuses on LCZ mapping and high-resolution temperature modelling. Together, these activities form a multi-scale framework linking atmospheric conditions, urban morphology, and thermal response, supporting improved urban environmental monitoring.

Keywords: Earth Observation, Air Quality, Urban Heat Island, Machine Learning

ИНТЕГРИСАНО ОСМАТРАЊЕ ЗЕМЉЕ И МЕТОДЕ ЗАСНОВАНЕ НА ПОДАЦИМА ЗА ПРАЋЕЊЕ КВАЛИТЕТА ВАЗДУХА И ТОПЛОТНОГ ОКРУЖЕЊА У УРБАНИМ СРЕДИНАМА

Сажетак:
Урбане средине су у све већој мјери изложене загађењу ваздуха и ефекту урбаног топлотног острва (УТО), што захтијева примјену интегрисаних приступа праћењу. У оквиру пројекта *Space It Up!*, овај рад представља усклађене истраживачке правце који комбинују податке Осматрања Земље (ОЗ) и методе засноване на подацима. Компонента квалитета ваздуха обухвата детекцију метана, интеграцију вишеизворних података и анализу недостатака у подацима са сателита Sentinel-5P, док се компонента топлотног комфора фокусира на картирање локалних климатских зона (ЛКЗ) и моделирање температуре високе просторне резолуције. Заједно, ове активности чине вишеразмјерни оквир који повезује атмосферске услове, урбану морфологију и топлотну реакцију, доприносећи унапређењу праћења животне средине у урбаним подручјима.

Кључне ријечи: Осматрање Земље, квалитет ваздуха, урбано топлотно острво, машинско учење

1. INTRODUCTION

Urban environments are increasingly exposed to multiple, interacting environmental stressors, requiring integrated monitoring approaches that combine atmospheric, climatic, and geospatial information. Within the framework of the Space It Up! project, funded by the Italian Space Agency (ASI) and the Ministry of University and Research (MUR), dedicated research activities have been developed within Spoke 7 to address these challenges through advanced Earth Observation (EO) and data-driven methodologies. In particular, we are presenting the work of two tasks focused on the main thematic domains: air quality (AQ) and urban heat island (UHI) and thermal comfort, which are investigated through complementary research lines spanning satellite data analysis, multi-source data integration, and high-resolution modelling. The AQ component addresses the limitations of satellite observations and the estimation of ground-level pollutant concentrations, while the UHI component focuses on the characterization of urban thermal patterns and their driving factors.

This work presents a set of coordinated research activities for urban environmental monitoring, developed within the same project framework but addressing distinct domains. In the air quality domain, a bivariate mapping approach is introduced to support methane screening by jointly considering exceedance frequency and observation availability, improving the interpretation of coarse-resolution satellite data. In parallel, an automated integration pipeline is developed to combine ground-based measurements, meteorological reanalysis, and satellite observations into a consistent dataset across Europe. A further contribution is the systematic analysis of Sentinel-5P data gaps, aimed at understanding their spatial and temporal structure and the environmental factors that drive missing observations.

Separately, in the urban climate domain, high-resolution air temperature modelling and Local Climate Zone mapping are applied to investigate the spatial variability of the urban heat island effect and its relationship with urban morphology. Additional analysis of surface composition using hyperspectral data provides further insight into the role of materials in shaping thermal behaviour. Although these research lines are developed independently, they collectively contribute to a broader perspective on urban environmental processes.

Within this context, the following sections present the main research lines developed in each domain, highlighting their methodological approaches and their role within a broader, integrated environmental monitoring framework.

2. AIR QUALITY

2.1. BIVARIATE MAPPING OF METHANE EXCEEDANCE AND OBSERVATION AVAILABILITY

Methane monitoring from space involves a trade-off between spatial resolution and observational coverage. Sentinel-5P provides continuous global observations with high temporal frequency but at coarse spatial resolution [1], limiting its ability to resolve individual emission sources. In contrast, hyperspectral instruments such as Planet's Tanager can detect and localize methane plumes at high spatial resolution [2], but with sparse temporal and spatial coverage. Sentinel-5P is primarily sensitive to larger emission sources, while hyperspectral sensors can detect smaller plumes [3]. In this context, the bivariate representation supports the analysis of co-visibility between Sentinel-5P methane signals and high-resolution plume detections, providing a first-order indication of where coarse-resolution observations capture underlying emission activity.

In this work, bivariate maps were developed to summarize two complementary aspects of the monthly Sentinel-5P methane signal: the number of valid observations available for each pixel and the number of times that pixel exceeded a selected methane threshold. The objective is to provide a screening and contextualization layer for Sentinel-5P methane observations, enabling the identification of candidate regions of interest that can be further analysed or validated using higher-resolution plume datasets such as Carbon Mapper.

2.1.1. Methodology

The workflow starts from monthly Sentinel-5P CH_4 observations over the study area. For each month, a raster of valid observation count is first computed, representing the number of usable methane retrievals available for each pixel after quality filtering. This layer describes the spatial distribution of data availability within the month.

A second raster is then derived for exceedance count, representing how many times the methane value at a given pixel exceeds a predefined threshold during the same monthly period. This layer provides a measure of how frequently elevated methane conditions are observed at each location.

The two rasters are then classified into ordinal classes and combined into a single categorical raster, producing the bivariate map. In this representation, one dimension corresponds to valid observations and the other to exceedance. Each final class therefore represents a specific combination of data availability and methane threshold occurrence.

2.1.2. Interpretation And Use

This formulation enables the joint assessment of signal strength and observational support, which is critical for distinguishing robust methane patterns from artefacts caused by sparse sampling. This makes it possible to compare spatial patterns more efficiently and to identify areas where methane exceedance and observational coverage occur in combination. The bivariate maps act as an intermediate screening layer, highlighting regions where Sentinel-5P indicates persistent methane signals supported by sufficient observational coverage. These regions can then be compared with high-resolution plume detections from Carbon Mapper (Tanager) to assess cross-sensor consistency and explore co-visibility between coarse and fine-scale observations.

A quantitative comparison with known methane plume detections from Carbon Mapper provides additional support for the effectiveness of the bivariate classification. Out of a total of 4,869 detected plumes, the distribution across exceedance classes is not uniform. Approximately 27.4% of plumes fall within classes characterized by high exceedance and sufficient observation availability, while 13.5% are associated with moderately high exceedance conditions. Lower proportions are observed for moderately low (17.9%) and low exceedance classes (37.7%). Overall, about 40.9% of plume detections are associated with higher exceedance classes, indicating that a substantial fraction of repeated methane enhancements captured by Sentinel-5P correspond to independently detected emission sources. In contrast, classes characterized by low exceedance or limited observation availability show a weaker correspondence with plume detections. This suggests that methane signals in these areas are either less persistent, of lower intensity, or not consistently captured by Sentinel-5P, highlighting the limitations of coarse-resolution observations under such conditions.

A further advantage of this approach is that it produces a consistent spatial framework for month-by-month comparison. Since both valid observations and exceedance are represented in the same product, the resulting maps can be used to evaluate how the spatial structure of methane-related patterns evolves over time. This is particularly useful in exploratory analyses where the interest is not limited to isolated detections but extends to broader recurring spatial behavior. This is especially relevant for Sentinel-5P data, where repeated observations provide temporal context that can help identify persistent emission patterns rather than isolated events.

These bivariate maps also support later processing steps. In particular, selected classes can be extracted and converted into vector polygons to define candidate regions of interest. These regions can then be used in downstream analyses, for example for spatial comparison with higher-resolution plume observations or for summarizing hotspot-like areas at monthly scale.

As an example, two locations may show similar exceedance counts during a month while differing in the number of valid observations available over that period. Representing both variables together allows these situations to be distinguished within the same map product. In this way, the bivariate formulation provides more information than a map based on exceedance alone.

Overall, the bivariate maps were designed as a simple and informative way to combine monthly methane exceedance and valid observation support into a unified representation. Their role in the workflow is to organize coarse-resolution Sentinel-5P information into a form that is easier to compare, interpret, and use in subsequent spatial analyses. Furthermore, the bivariate maps provide a practical first-stage screening tool for methane analysis, enabling the identification of priority regions for further investigation. These regions can then be analysed in greater detail using Sentinel-5P time series and methane enhancement techniques (e.g., ΔXCH_4, background subtraction, anomaly detection), or cross-compared with high-resolution plume observations, supporting a multi-scale approach to methane detection and monitoring.

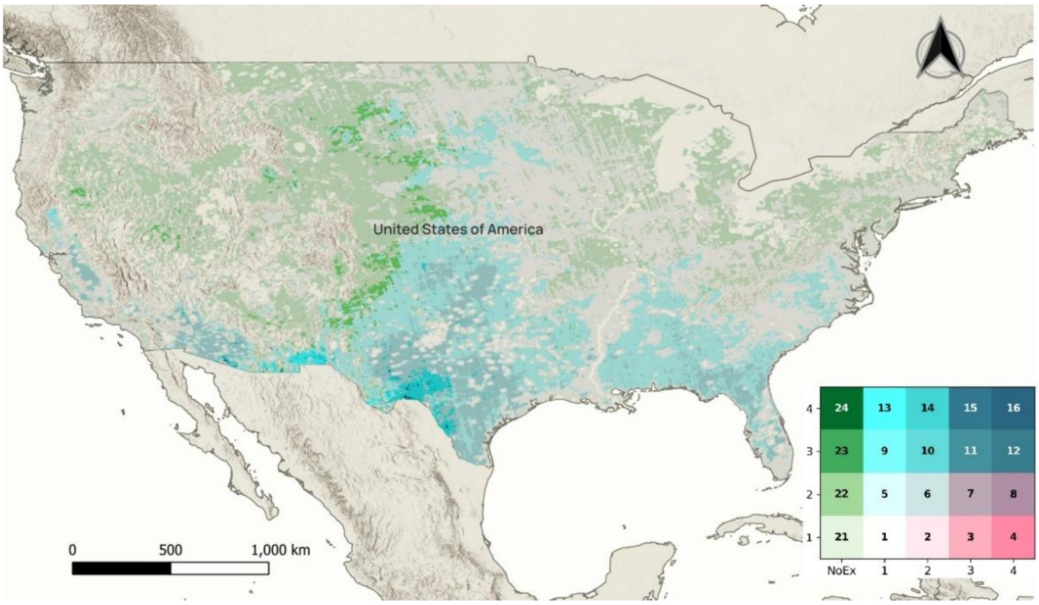

Figure 1. *Example of a monthly bivariate map for January 2023 over CONUS. In the legend, the x-axis shows the exceedance class E_c from low to high, with NoEx denoting zero exceedance, while the y-axis shows the valid-observation class V_c from low to high. Each color represents one joint class combining the two variables, based here on custom bins applied to the monthly raw counts.*

2.2. AUTOMATED INTEGRATION FRAMEWORK FOR AIR QUALITY AND METEOROLOGICAL DATA ACROSS EUROPE

2.2.1. Overview and Motivation

Urban air quality is shaped by a complex interplay of emission sources, atmospheric dynamics, and meteorological conditions. Ground-based monitoring networks, while essential, are inherently limited in their spatial coverage: sensors can only capture local concentrations at fixed locations, leaving large portions of urban and peri-urban areas uncharacterized. At the same time, pollutant concentrations are highly sensitive to wind patterns, boundary layer height, temperature gradients, and precipitation, factors that vary continuously across space and time [4]. This creates a fundamental tension between the point-scale precision of ground sensors and the spatially continuous information needed for robust environmental assessment.

To bridge this gap, this research integrates three complementary data sources, ground-level air quality sensors from the European Environment Agency (EEA), meteorological reanalysis fields from ERA5, and satellite tropospheric column retrievals from Sentinel-5P/TROPOMI, into a single, harmonized dataset covering a user-defined area across Europe. The objective is to enable the estimation and analysis of ground-level pollutant concentrations by jointly leveraging in-situ observations, meteorological drivers, and satellite-derived information. The resulting unified record links each observation point with its corresponding atmospheric context in space and time, providing a foundation for data-driven modelling of air quality and complementing existing satellite-based surface estimation approaches [5], [6], [7].

2.2.2. Exploratory Analysis of EEA Data

The first component of this work focuses on understanding the EEA air quality dataset before any integration takes place. The EEA Discomap Download Service provides access to daily and hourly measurements from thousands of monitoring stations across Europe, reported by member states under Directive 2008/50/EC. Rather than simply downloading raw data, this step builds an analytical layer that allows the user to interrogate the dataset interactively: selecting countries, pollutants, and time periods, then visualizing trends, seasonal patterns, and cross-country comparisons.

A critical aspect of working with EEA data is understanding its two temporal series. Verified data, covering 2013 through 2024, has undergone full quality assurance review before submission by national agencies. Near-real-time data, available from 2025 onwards, is transmitted continuously but may still contain uncorrected anomalies. Distinguishing between these two series matters for any analysis that mixes historical and recent observations, so the selection is made automatically based on the period requested by the user.

2.2.3. Building The Integrated Dataset

The integration pipeline begins with the same EEA station catalogue used in the exploration analysis but now applies a spatial filter to retain only the sensors that fall within the user-defined area of interest. This bounding box can cover a single city, a metropolitan region, or an entire country, making the framework applicable at multiple scales without any structural change to the code.

A central challenge in merging datasets from different sources is that they do not share a common spatial grid. EEA sensors are distributed irregularly across the landscape, following historical decisions about where to place monitoring equipment. ERA5, by contrast, provides data on a regular 0.25-degree global grid. To reconcile these geometries, a custom interpolation grid is constructed from the sensor locations themselves: the minimum distance between any two stations is computed, and a regular grid is generated at 90% of that spacing. This choice balances spatial coverage and resolution, ensuring that the grid reflects the effective density of the monitoring network without introducing excessive interpolation artefacts. It is slightly finer than the sensor network, which ensures that every station falls within at least one grid cell and that no observations are lost during the spatial join. Because not all sensors measure the same pollutants every day, this minimum distance is recalculated for each pollutant and date range, so the grid always reflects the actual spatial density of available observations.

With the grid defined, ERA5 meteorological variables are interpolated onto the sensor locations using bilinear interpolation. This is done for each hour of the analysis period, covering temperature, surface pressure, boundary layer height, wind speed, solar and thermal radiation, and total precipitation. The boundary layer height is particularly relevant because it governs how efficiently the atmosphere dilutes surface emissions: a shallow boundary layer traps pollutants near the ground, while a deep one allows them to disperse vertically. By including this variable alongside the pollutant concentrations, the dataset captures the meteorological mechanism behind pollution episodes.

Measurements are then organized into two temporal windows that bracket the Sentinel-5P satellite overpass: a previous window covering the hours before the overpass, and a current window aligned with the satellite's observation time over the area. This synchronization is essential because Sentinel-5P measures the total column of pollutants integrated through the atmosphere, which reflects conditions at the time of the overpass rather than a daily average. Computing the mean ground-level concentration for the same window ensures physical consistency between ground and satellite observations.

Sentinel-5P data are extracted from the Google Earth Engine archive using adaptive circular buffers around each station. The buffer radius scales with the grid resolution so that it captures enough satellite pixels to ensure a statistically stable estimate while preserving spatial representativeness. Because cloud cover or unfavorable overpass geometry may mean no satellite data exists for a given station on a given day, missing values are retained explicitly in the final dataset rather than being removed, allowing downstream analysis to account for data availability.

The three streams, EEA ground concentrations, ERA5 meteorological variables, and Sentinel-5P column densities, are finally joined by matching station coordinates and dates. Negative concentration values, which can result from sensor noise or calibration drift, are flagged and removed, and the cleaned dataset is exported as a structured table. Table 1 shows a representative excerpt of the final output, where each row corresponds to one station on one day and carries measurements from all three sources simultaneously.

Table 1. Sample rows from the integrated output. Each record combines ground sensor concentration, ERA5 meteorological context, and Sentinel-5P column density at the same location and time. S5P values of NaN indicate no satellite overpass was available for that station and date.

Date	Station	Pollutant	Prev (µg/m³)	Curr (µg/m³)	S5P (mol/m²)	T (°C)
2025-10-01	IT_MI_001	NO_2	16.54	22.30	1.11e-4	15.4
2025-10-01	IT_MI_003	NO_2	66.04	48.10	NaN	14.9
2025-10-02	DE_MUC_41	NO_2	21.80	19.20	9.70e-5	12.1
2025-10-02	ES_MAD_07	NO_2	38.50	44.70	1.43e-4	18.6

Overall, the integration framework addresses key limitations of individual data sources by combining the spatial coverage of satellite observations, the temporal continuity of meteorological reanalysis, and the accuracy of ground-based measurements.

2.3. EXPLORATORY ANALYSIS OF SENTINEL-5P DATA GAPS

Satellite-based air quality monitoring using Sentinel-5P provides daily global observations of trace gases such as NO_2 and SO_2 [1], but its practical use is substantially limited by spatio-temporal data gaps. These gaps arise from cloud contamination, surface reflectance effects, viewing geometry constraints, and strict quality assurance (QA) filtering, and can severely reduce the reliability of downstream applications such as emission assessment, exposure analysis, and time-series interpretation [1].

To address this limitation, it is necessary to first characterise the structure and drivers of missing observations before applying any reconstruction or modelling approach. In this work, a gap is defined as any S5P pixel-day that is missing or invalid after QA filtering [1], [8]. Starting from daily multi-band images (one band per day), we construct a binary gap mask $G(t,x)$ and summarise it across time and space to quantify how often, when, and where gaps occur, and how they differ between NO_2 and SO_2.

This exploratory analysis provides a diagnostic understanding of missingness patterns, including their seasonal behaviour, temporal evolution, and dependence on environmental factors. Such characterization is essential for determining whether missingness is random or systematically linked to observation conditions, and for guiding the design of subsequent modelling or gap-filling strategies.

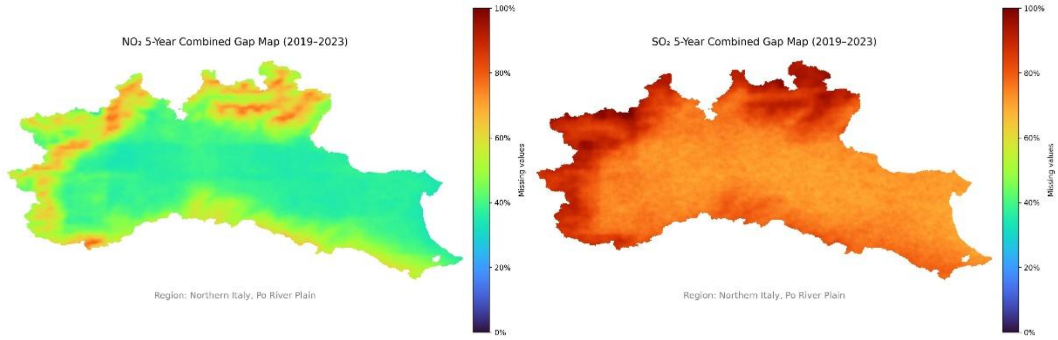

Figure 2. *NO_2 and SO_2 Year Gap Maps (2019-2023) (created by author).*

2.3.1. NO_2 And SO_2 Seasonal Data Gaps Pattern

Seasonal patterns were derived by aggregating daily coverage into four fixed seasons: DJF (December–February), MAM (March–May), JJA (June–August), and SON (September–November). For each species and season, the pixel-wise seasonal data gap ratio was computed as the fraction of days classified as missing-defined as days with values = 0 or NaN-within that season, and then summarized over the AOI. This enables the assessment of seasonal biases in data availability, which are expected due to cloud cover and solar geometry effects.

Overall, data gaps are substantial and differ markedly between species. NO_2 exhibits moderate missingness (NO_2 ~45%), while SO_2 shows consistently high data gaps (~77%) across all seasons, with particularly severe loss in winter months. This effect is further amplified at mid-latitudes during winter, when high solar zenith angles reduce the signal-to-noise ratio of satellite retrievals, leading to more stringent QA filtering and increased data gaps, particularly for SO_2. This highlights the greater difficulty of reconstructing SO_2 fields and the need for stronger reliance on auxiliary information. The observed seasonal pattern, with higher missingness in winter and lower in summer, is consistent with increased cloud cover and unfavourable solar geometry during winter months, which limit retrieval quality.

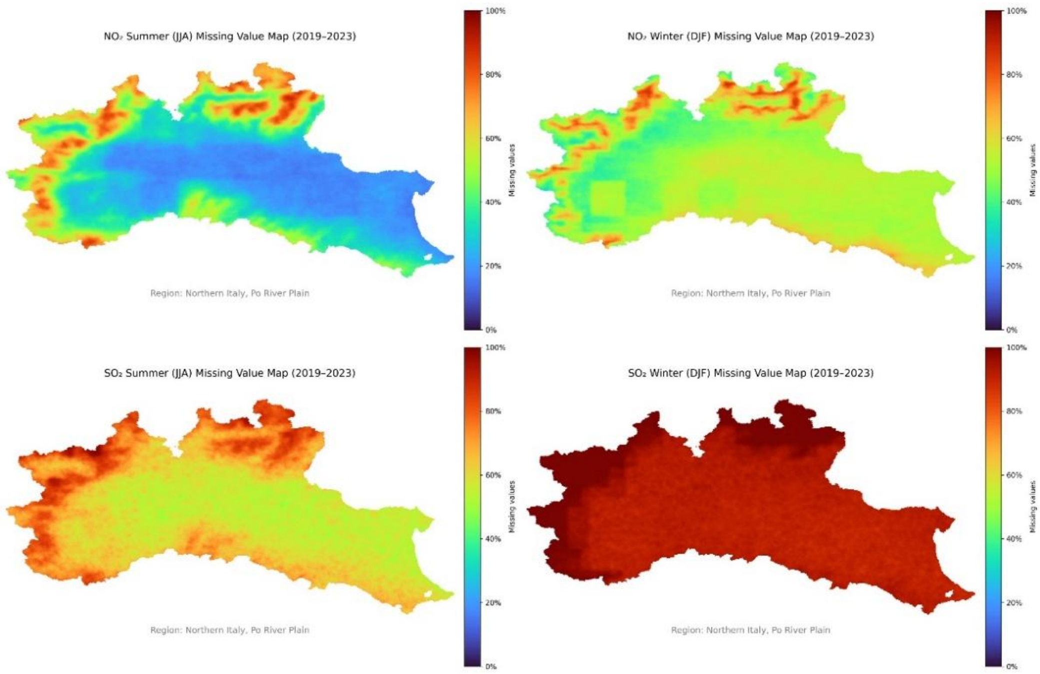

Figure 3. NO_2 and SO_2 Seasonal Gap Maps (2019-2023) (created by author).

2.3.2. Interannual Trends in No_2/So_2 Data Gaps

Interannual trends were analysed at the pixel level for both NO_2 and SO_2 over 2019−2023. Annual data gap ratios were computed as the fraction of days with non-positive or NaN values. These yearly maps were stacked to form a time series at each pixel, and monotonic trends were assessed using the Mann−Kendall test, with Sen′s slope used to estimate the rate of change. Positive slopes indicate increasing data gaps, while negative slopes indicate decreasing gaps. We report slope, p-value, and significance ($p < 0.05$) maps. Overall, interannual trends are weak and spatially sparse, with only ~3.2% of pixels showing statistically significant trends, suggesting that missingness is largely driven by persistent observational constraints rather than systematic long-term changes.

2.3.3. Correlation Between Elevation and No_2/So_2 Data Gaps

Motivated by persistent spatial patterns of high data gap ratios (notably along the western AOI), we examined whether terrain elevation helps explain this variability.

For each species, daily observations (2019–2023) were aggregated to a per-pixel data gap ratio, then compared with elevation after resampling to a common grid. Using all valid pixels ($n = 94{,}666$), we computed both Pearson and Spearman correlations to quantify linear relationships between elevation and data gaps.

The strong positive correlation (r up to ~0.92) between elevation and data gaps indicates that complex terrain is associated with higher missingness, likely due to orographic cloud formation and viewing geometry effects.

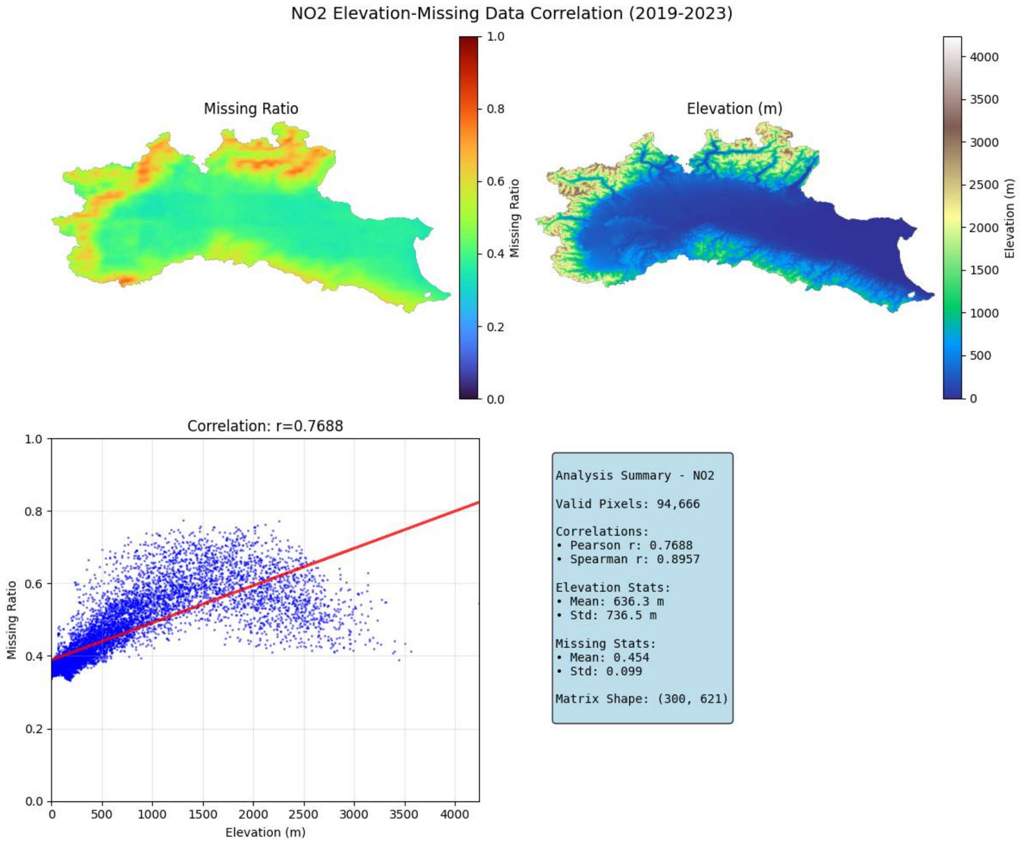

Figure 4. NO_2 Data Gaps-Elevation Correlation (created by author).

2.3.4. Correlation Between Cloudiness and No_2/So_2 Data Gaps

In this section, daily cloud fraction was retrieved from Sentinel-5P (TROPOMI) in Google Earth Engine for 2019–2023, using the same AOI and grid as the NO_2 and SO_2 products. Cloud fraction is in [0, 1] and denotes the share of a pixel covered by cloud (0 cloud-free, 1 fully cloud-covered).

The pollutant and cloud datasets were then co-registered, and for each pixel we computed (1) the five-year data gaps ratio of the pollutant (count of days with value = 0 or NaN divided by total days in 2019–2023) and (2) the five-year mean cloud fraction, averaging over valid cloud observations at that pixel (ignoring NaNs). We then evaluated pixel-wise Pearson and Spearman correlations between data gaps and cloudiness.

Diagnostics include a map of pollutant data gaps, a map of mean cloud fraction, and a hexbin plot of cloud fraction versus data gaps with a fitted linear trend. Because SO_2 cloud fractions in the AOI are very small, the SO_2 hexbin uses an x-axis of 0 to 0.1 for readability, while NO_2 uses 0 to 1. This workflow provides AOI-wide correlation summaries together with spatial and distributional context.

This analysis helps distinguish whether cloud cover is a primary driver of missingness or whether other factors, such as retrieval filtering or low signal conditions, dominate.

For NO_2, the positive correlation confirms that cloud cover is a major driver of missingness. In contrast, SO_2 gaps remain high even under low cloud fractions, indicating that additional factors–such as stricter QA filtering and low signal-to-noise conditions–play a dominant role.

In summary, data gaps in Sentinel-5P NO_2 and SO_2 products are substantial, structured, and strongly dependent on season, topography, and atmospheric conditions. These findings indicate that missingness is not random, but instead driven by physical and observational processes, including cloud cover, topography, and retrieval constraints such as high solar zenith angles. Consequently, effective gap-filling approaches must explicitly incorporate spatio-temporal context and auxiliary predictors, rather than relying on simple interpolation. The pronounced differences between NO_2 and SO_2 further suggest that pollutant-specific modelling strategies are required.

3. URBAN HEAT ISLAND AND THERMAL COMFORT

Global warming is driving a significant increase in extreme heat events, with substantial impacts on both natural ecosystems and human systems [9]. In Europe, and particularly in the Mediterranean basin, these phenomena are especially pronounced, as this region is recognised as a climate change hotspot [10]. Over recent decades, the intensification of heatwaves (HWs) has led to a marked rise in heat-related mortality, particularly affecting vulnerable population groups such as the elderly and individuals with pre-existing health conditions [11]. In this context, understanding the spatial and temporal dynamics of heat exposure, especially in urban areas where the urban heat island (UHI) effect exacerbates thermal stress, is key to developing effective mitigation and adaptation strategies.

In this context, Task 7.4.2 addresses the growing impacts of UHI under increasing HW frequency, duration, and intensity. The Task focuses on urban and suburban environments, with the ultimate goal of improving the understanding, monitoring, and modelling of urban thermal patterns and their driving factors. The activities are structured around four research lines, as described in the following sections.

3.1. RECENT CLIMATE TRENDS AND THERMAL STRESS ASSESSMENT

A first research line focuses on the analysis of recent climate variability and trends across Italy, with a focus on HWs and thermal stress conditions. For this purpose, a very-high-resolution climate reanalysis dataset (VHR-REA_IT, 2.2 km), developed by the Euro-Mediterranean Centre on Climate Change (CMCC) [12], is exploited in combination with authoritative observations from the synoptic network of the Italian Air Force Meteorological Service. The integration of these datasets allows both the validation of reanalysis products and a detailed investigation of spatial variability at the national scale.

The analysis covers the period 1981-2024 (44 years). Trends are estimated using linear regression and examined across different territorial units, including ecoregions and elevation ranges, to account for the influence of topography and land characteristics. The study involves daily maximum and minimum temperature extremes, standard climate indices defined by the Expert Team on Climate Change Detection and Indices (ETCCDI), and thermal stress indicators that combine air temperature and relative humidity.

The results reveal a clear and spatially coherent warming signal across Italy. In particular, there is a widespread increase in warm extremes and a decrease in cold extremes. Tropical nights (minimum temperature above 20 °C) show the most pronounced and consistent increase, reaching up to approximately +7 days per decade. HW frequency also exhibits a significant upward trend, with an average increase of about +2 events per decade.

The analysis of thermal stress highlights a substantial intensification of discomfort conditions during the warm season. These trends are not limited to daytime but extend into nighttime and early morning hours, in line with the observed increase in tropical nights. The most pronounced trends are found in lowland and densely populated areas, indicating a growing exposure of urban populations to heat-related risks.

3.2. MAPPING LOCAL CLIMATE ZONES USING HYPERSPECTRAL DATA

Another activity regards the classification of urban environments into Local Climate Zones (LCZs), a standard framework that divides urban and suburban areas into classes based on their morphology and land cover composition [13]. The LCZ system is widely adopted for assessing the UHI intensity and interpreting spatial variations in temperature across urban environments.

The project relies on the methodology proposed in [14], which integrates hyperspectral PRISMA imagery, multispectral Sentinel-2 data, and urban canopy parameter (UCP) layers. These parameters include, e.g. building height, impervious surface fraction, and sky view factor, which are key descriptors of the urban structure.

The methodology has been successfully applied to multiple urban areas worldwide, including Milan and Rome (Italy), and Hanoi and Ho Chi Minh City (Vietnam), demonstrating its transferability across diverse climatic and morphological contexts.

Ongoing developments focus on further automating critical steps in the pipeline, such as data retrieval, training, and test sample generation. In particular, the project aims to streamline the selection and quality control of training and testing polygons, which represent the most critical and subjective step of the workflow. This process is guided by criteria related to polygon geometry, class balance, and distribution of UCPs per class, ensuring robust model training and improved classification accuracy. These improvements are expected to foster large-scale applications and support comparative studies across cities.

3.3. HIGH-RESOLUTION AIR TEMPERATURE MODELLING

A second research line focuses on modelling the spatial distribution of near-surface air temperature at high resolution within urban areas. This activity integrates in situ measurements from both official and crowdsourced meteorological networks with geospatial and Earth Observation (EO) predictors through a machine learning technique.

A Random Forest regression framework is employed to generate 20 m resolution air temperature maps over the city of Milan for the year 2022. The analysis focuses on HW periods identified from the long-term reanalysis dataset and considers multiple times of day to capture the diurnal evolution of the UHI effect. The modelling framework is based on a dataset of 97 measurement stations and incorporates a range of predictors derived from geospatial and EO data, including spectral indices from Sentinel-2 imagery and metrics describing urban morphology.

Model performance varies across the diurnal cycle, with the highest accuracy achieved during late afternoon and nighttime periods. The coefficient of determination ranges between 0.33 and 0.37, while the root mean square error is between 0.7 and 1.4 °C. Although these values indicate moderate agreement with observations, they are consistent with the challenges of modelling air temperature at such fine spatial resolution, especially during daytime.

Despite these challenges, the resulting high-resolution maps effectively capture the spatial heterogeneity of urban temperatures (see Figure 5b). In fact, a pronounced UHI effect is clearly identified, with central urban areas exhibiting temperatures up to 3-5 °C higher than the surrounding zones. At the same time, urban green spaces such as parks provide a measurable cooling effect, on the order of 1-2 °C. Additionally, a clear relationship between LCZs and air temperature is noticed (Figure 5). Compact built-up classes (namely LCZ 2, LCZ 3 and LCZ 8) indicate higher urban heat load. On the contrary, less dense built-up areas (for example, LCZ 5 and LCZ 6), along with many natural classes (such as LCZ 101 and LCZ 102), show lower air temperatures. The results show that high-resolution air temperature maps have clear practical uses. They also suggest that LCZs can help identify urban areas with higher heat risk, which is key when assessing how people are exposed to heat.

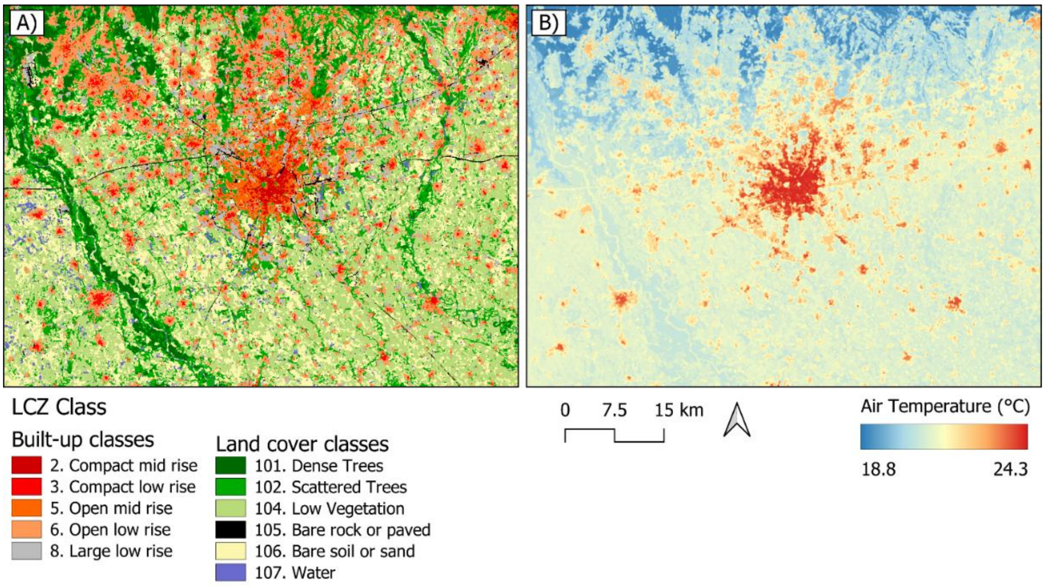

Figure 5. LCZ map of Milan for June 2022 (left panel) and air temperature map during maximum UHI (MUHI) phase (corresponding to 2 hours before sunrise) for June 2022 HW (right panel) (created by author).

3.4. URBAN SURFACE COMPOSITION AND THERMAL RESPONSE

The last research line investigates the relationship between urban surface composition and thermal behaviour through hyperspectral unmixing techniques. Hyperspectral images from the PRISMA and DESIS missions are used to estimate the fractional abundance of different surface materials, which are ultimately related to the land surface temperature (LST) derived from Landsat 8/9 thermal infrared (TIR) data.

A constrained spectral unmixing approach is applied to ensure physically consistent results, with material fractions constrained to be non-negative and to sum to one for each pixel. The analysis focuses on materials that are particularly relevant for urban climate, including artificial surfaces such as asphalt, shingle and metal, as well as natural components such as bare soil, vegetation (both tall and low), and water.

The derived material fractions provide a detailed representation of urban surface composition, which is then compared with LST measurements and the high-resolution air temperature maps generated through the machine learning framework described above. Figure 6 shows LST distributions across fraction quartiles for four surface materials. Shingles and asphalt both increase LST, with asphalt showing a stronger effect, likely due to its low albedo and low thermal capacity, which cause it to heat up quickly and retain heat throughout the day. Tall and low vegetation, on the other hand, reduce LST, with tall vegetation having a slightly larger cooling effect, possibly due to greater evapotranspiration and shading. This integrated analysis enables the investigation of how different materials contribute to surface heating and cooling processes, and how these effects propagate to near-surface air temperature.

Furthermore, validation activities are being conducted using high-resolution hyperspectral and thermal data acquired during an aerial survey over Milan on 15-16 August 2025. Additional comparisons are performed using near-simultaneous multispectral data and reference geospatial datasets, with the goal of assessing the quality of the spectral unmixing result.

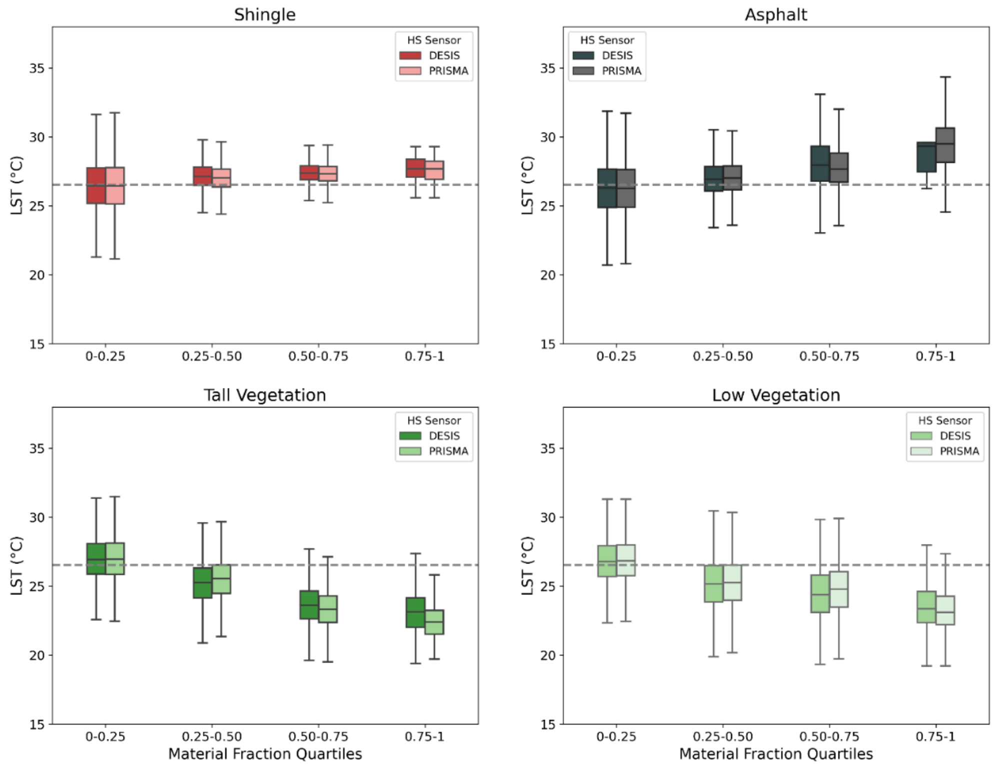

Figure 6. Boxplots of LST distributions per surface material abundance classes derived from PRISMA and DESIS data. Distributions are grouped by material abundance quartiles (ranging from 0 to 100%). Grey horizontal line indicates mean LST value (created by author).

4. CONCLUSIONS

This work presents a set of complementary research lines addressing urban air quality and thermal environment, developed within a common project context but following distinct methodological approaches. In the air quality domain, the results show that combining multiple data sources improves the characterization of atmospheric conditions, while the analysis of Sentinel-5P data gaps confirms that missing observations are structured and driven by environmental and observational factors. The proposed bivariate mapping approach provides a practical tool for methane screening, enabling a more informed interpretation of coarse-resolution satellite signals.

In parallel, the urban climate investigations highlight the strong spatial variability of thermal conditions within cities. High-resolution temperature modelling captures the urban heat island effect and its relationship with Local Climate Zones, while hyperspectral analysis of surface composition provides further insight into the role of materials in controlling surface and air temperature patterns. Although developed as separate research lines, these activities contribute to a broader understanding of urban environmental dynamics, where atmospheric composition and thermal processes are both influenced by spatial structure and environmental conditions. Future work may focus on strengthening the quantitative evaluation of the proposed methods and extending their application across different cities and datasets.

AKCNOWLEDGEMENTS

This study was carried out within the Space It Up project funded by the Italian Space Agency, ASI, and the Ministry of University and Research, MUR, under contract n. 2024-5-E.0 – CUP n. I53D24000060005.

LITERATURE

[1] J. P. Veefkind et al., "TROPOMI on the ESA Sentinel-5 Precursor: A GMES mission for global observations of the atmospheric composition for climate, air quality and ozone layer applications," Remote Sensing of Environment, vol. 120, pp. 70–83, May 2012, doi: https://doi.org/10.1016/j.rse.2011.09.027.

[2] A. K. Thorpe et al., "Attribution of individual methane and carbon dioxide emission sources using EMIT observations from space," Science Advances, vol. 9, no. 46, Nov. 2023, doi: https://doi.org/10.1126/sciadv.adh2391.

[3] B. J. Schuit et al., "Automated detection and monitoring of methane super-emitters using satellite data," Atmospheric Chemistry and Physics, vol. 23, no. 16, pp. 9071–9098, Sep. 2023, doi: https://doi.org/10.5194/acp-23-9071-2023.

[4] Z. Mushtaq et al., "Satellite or ground-based measurements for air pollutants (PM2.5, PM10, SO2, NO2, O3) data and their health hazards: which is most accurate and why?," Environmental monitoring and assessment, vol. 196, no. 4, Mar. 2024, doi: https://doi.org/10.1007/s10661-024-12462-z.

[5] J. R. Cedeno Jimenez and M. A. Brovelli, "NO2 Concentration Estimation at Urban Ground Level by Integrating Sentinel 5P Data and ERA5 Using Machine Learning: The Milan (Italy) Case Study," Remote Sensing, vol. 15, no. 22, Nov. 2023, Art. no. 5400, doi: https://doi.org/10.3390/rs15225400.

[6] M. A. Brovelli, J. R. Cedeno Jimenez, A. Moazzam, V. Yordanov, and A. Vavassori, "Remote Sensing and Machine Learning for Urban Air Quality and Heat Island Monitoring," The International Archives of the Photogrammetry, Remote Sensing and Spatial Information Sciences, vol. XLVIII-4/W142025, pp. 3–10, Nov. 2025, doi: https://doi.org/10.5194/isprs-archives-xlviii-4-w14-2025-3-2025.

[7] Z. Liang, J. R. Cedeno Jimenez, V. Yordanov, and M. A. Brovelli, "Estimating Ground-Level Carbon Monoxide Concentrations Using Machine Learning Techniques: The Metropolitan City of Milan Case Study," The International Archives of the Photogrammetry, Remote Sensing and Spatial Information Sciences, vol. XLVIII-4/W182025, pp. 241–248, Jan. 2026, doi: https://doi.org/10.5194/isprs-archives-xlviii-4-w18-2025-241-2026.

[8] D. Loyola et al., "The operational cloud retrieval algorithms from TROPOMI on board Sentinel-5 Precursor," vol. 11, no. 1, pp. 409–427, May 2017, doi: https://doi.org/10.5194/amt-11-409-2018.

[9] S. Campbell, T. A. Remenyi, C. J. White, and F. H. Johnston, "Heatwave and health impact research: A global review," Health & Place, vol. 53, no. 53, pp. 210–218, Sep. 2018, doi: https://doi.org/10.1016/j.healthplace.2018.08.017.

[10] F. Giorgi, "Climate change hot-spots," Geophysical Research Letters, vol. 33, no. 8, 2006, doi: https://doi.org/10.1029/2006gl025734.

[11] J. Ballester et al., "Heat-related mortality in Europe during the summer of 2022," Nature Medicine, vol. 29, no. 29, pp. 1–10, Jul. 2023, doi: https://doi.org/10.1038/s41591-023-02419-z.

[12] M. Raffa et al., "VHR-REA_IT Dataset: Very High Resolution Dynamical Downscaling of ERA5 Reanalysis over Italy by COSMO-CLM," Data, vol. 6, no. 8, Aug. 2021, Art. no. 88, doi: https://doi.org/10.3390/data6080088.

[13] I. D. Stewart and T. R. Oke, “Local Climate Zones for Urban Temperature Studies,” Bulletin of the American Meteorological Society, vol. 93, no. 12, pp. 1879–1900, Dec. 2012, doi: https://doi.org/10.1175/bams-d-11-00019.1.

[14] A. Vavassori et al., “A combined Remote Sensing and GIS-based method for Local Climate Zone mapping using PRISMA and Sentinel-2 imagery,” International Journal of Applied Earth Observation and Geoinformation, vol. 131, pp. 103944–103944, Jun. 2024, doi: https://doi.org/10.1016/j.jag.2024.103944.